
EXPERIMENTAL ONLINE QUANTUM DOTS CHARGE AUTOTUNING USING NEURAL NETWORKS

A PREPRINT

✉ **Victor Yon**^{*1,2,3}, ✉ **Bastien Galaup**^{1,2,3}, ✉ **Claude Rohrbacher**^{2,3,4}, **Joffrey Rivard**^{2,3,4}, **Alexis Morel**^{2,3,4},
✉ **Dominic Leclerc**^{2,3,4}, ✉ **Clément Godfrin**⁵, ✉ **Ruoyu Li**⁵, **Stefan Kubicek**⁵, ✉ **Kristiaan De Greve**⁵,
Eva Dupont-Ferrier^{2,3,4}, ✉ **Yann Beilliard**^{1,2,3}, ✉ **Roger G. Melko**^{6,7}, and ✉ **Dominique Drouin**^{1,2,3}

¹Institut Interdisciplinaire d’Innovation Technologique (3IT), Université de Sherbrooke, Sherbrooke, QC, Canada, J1K 0A5

²Laboratoire Nanotechnologies Nanosystèmes (LN2) — CNRS 3463, Université de Sherbrooke, Sherbrooke, QC, Canada, J1K 0A5

³Institut quantique (IQ), Université de Sherbrooke, Sherbrooke, QC, Canada, J1K 2R1

⁴Département de physique, Université de Sherbrooke, Sherbrooke, QC, Canada, J1K 2R1

⁵IMEC, Kapeldreef 75, 3001 Leuven, Belgium

⁶Department of Physics and Astronomy, University of Waterloo, Waterloo, ON, Canada, N2L 3G1

⁷Perimeter Institute for Theoretical Physics, Waterloo, ON, Canada, N2L 2Y5

February 13, 2025

ABSTRACT

Spin-based semiconductor qubits hold promise for scalable quantum computing, yet they require reliable autonomous calibration procedures. This study presents an experimental demonstration of online single-dot charge autotuning using a convolutional neural network integrated into a closed-loop calibration system. The autotuning algorithm explores the gates’ voltage space to localize charge transition lines, thereby isolating the one-electron regime without human intervention. This exploration leverages the model’s uncertainty estimation to find the appropriate gate configuration with minimal measurements while reducing the risk of failures. In 20 experimental runs, our method achieved a success rate of 95 % in locating the target electron regime, highlighting the robustness of this approach against noise and distribution shifts from the offline training set. Each tuning run lasted an average of 2 hours and 9 minutes, primarily due to the limited speed of the current measurement. This work validates the feasibility of machine learning-driven real-time charge autotuning for quantum dot devices, advancing the development toward the control of large qubit arrays.

Keywords quantum dot · spin qubit · machine learning · convolutional neural network · scalable quantum computing · autonomous calibration · charge autotuning

1 Introduction

Semiconductor spin qubits [1–5] can encode quantum information using the spin- $1/2$ of a charge carrier, which can be manipulated using external magnetic fields to perform quantum computing based on the principles of superposition and entanglement. This technology stands out due to its high gate fidelity [6–12], long coherence times [13, 14], thermal robustness [15–17], and compatibility with existing complementary metal-oxide-semiconductor (CMOS) technologies [18–22]. These characteristics make spin qubits excellent candidates for building scalable quantum computers using already existing industrial fabrication methods [22–25]. However, significant engineering challenges remain, such as improving device fabrication quality [26–29] and developing autonomous calibration procedures for a large number of quantum dots (QDs) [30, 31].

*victor.yon@usherbrooke.ca

A spin qubit is formed by trapping a specific number of charge carriers within an isolated island (QD) using, for example, the electrostatic confinement gates of a nanoscale device (as shown in Figure 1a). Calibrating the QD device to achieve a specific physical state is a complex task that is generally approached in a series of sequential steps [32]. Initially, the device is cooled, local charge sensing systems are activated, and the voltages of the confinement gates are adjusted to operate within appropriate ranges for data collection [33, 34]. Following this, the gate voltage ranges corresponding to a known global structure (such as single- or double-QD configurations) are calibrated. This step is usually referred to as coarse tuning [35–42]. Next, optional virtual gates could be established to compensate for capacitive crosstalk, ensuring precise control of the individual QDs without unwanted interference [35, 36, 43–47]. Subsequently, the device gate voltages are precisely tuned to achieve a specific charge carrier count in each QD, which in our experiment refers to the number of electrons in a single QD. This step is usually referred to as charge state tuning [35, 48–54]. Finally, the system’s physical parameters are refined in preparation for quantum computations [36, 55–57].

Performing efficient and accurate calibration every time the system is cooled down is critical to deploying large-scale QD-based systems. However, automatizing this process is challenging due to the sensitivity of the operational parameters, where each variable can affect others nonlinearly, exponentially increasing the complexity as the number of tuned devices grows. Variability in device fabrication adds another layer of difficulty, as each QD can behave differently, requiring customized tuning approaches. These devices and the measurement method are also susceptible to environmental conditions (e.g., thermal noise and electromagnetic interference), adding stochasticity to the measurements.

Recent progress in producing larger arrays of QDs [24, 30] has accelerated the need for robust control procedures. This challenge has been partially addressed by leveraging machine learning (ML) models [38, 40], which can be used to tune quantum devices by automatically navigating through the large and noisy parameter space. However, ML methods, especially neural networks (NNs), are sensitive to the distribution shift [58] between the training and testing data and are well known for unexpected failures [59]. Therefore, it is necessary to validate any NN-based autotuning method in a real-world experimental environment [33]. However, due to the scarcity and expense of the hardware required to run such experiments, most autotuning demonstrations are performed offline (i.e., using static pre-recorded data). A few studies have demonstrated online experimental procedures for the first steps of the autotuning process: bootstrapping [33], coarse tuning [37, 42], and creating virtual gates [45, 46]. Baart et al. [53] showed an early demonstration of charge state autotuning using Gabor filters [60] and classical optimization algorithms, resulting in a single successful run after 3 hours. Only Schuff et al. [61] ran and benchmarked online experiments that covered the full tuning procedure. Their method—based on a combination of tree search, Bayesian optimization, segmentation algorithms, and NNs—allowed them to reach 77% success over 13 runs for complete QD tuning. However, each run took an average of 38 hours to complete due to the time required to measure large stability diagrams and the repeated calibration necessary after a stage failure.

The autotuning algorithm used during the experiment has been developed and tested offline in a previous study [51]. It relies on a convolutional neural network (CNN) [62–64] trained to detect charge transition lines in a small section of the stability diagram. The training is performed in a supervised manner on a dataset [65] composed of static measurements made on similar silicon QD devices. Then, a closed-loop calibration procedure allows us to find the one-electron regime of a single QD by following an autonomous exploration strategy that leverages the CNN inference and uncertainty score. Exploiting the model’s uncertainty improves the robustness of the autotuning by reducing the risk of critical failures caused by potential misclassifications [51] compared to classical ML methods [32, 48].

In this experiment, we successfully transfer the above ML-based charge autotuning method—developed using offline measurements—to real-time charge tuning on an experimental setup. The results confirm that the device-to-device variability and the resolution shift between the online and offline data do not negatively affect the line detection performance. We were also able to measure valuable information regarding the autotuning duration and identify the current measurement as the time bottleneck.

2 Methodology

The charge tuning process is typically guided by a stability diagram (two-dimensional current–voltage scan presented in Figure 3a), which is generated based on indirect QD measurements from a single-electron transistor (SET) for charge detection while sweeping the gate voltages. The transition lines (highlighted in green in Figure 3c) inform us of an electron movement between the reservoir and the QD (represented in Figure 1a,b). Given the knowledge that the QD is empty when no lines are visible at low gate voltages, it is possible to deduce the number of charges for a given position in the stability diagram (blue areas in Figure 3c). Although experts can perform manual tuning in small-scale experiments [54], this is too slow and labor-intensive for large-scale industrial applications utilizing multiple QDs. Automating this task is necessary but challenging due to the noise induced by the environment and the measurement electronics, the device-to-device variability, and the variety of existing hardware implementations.

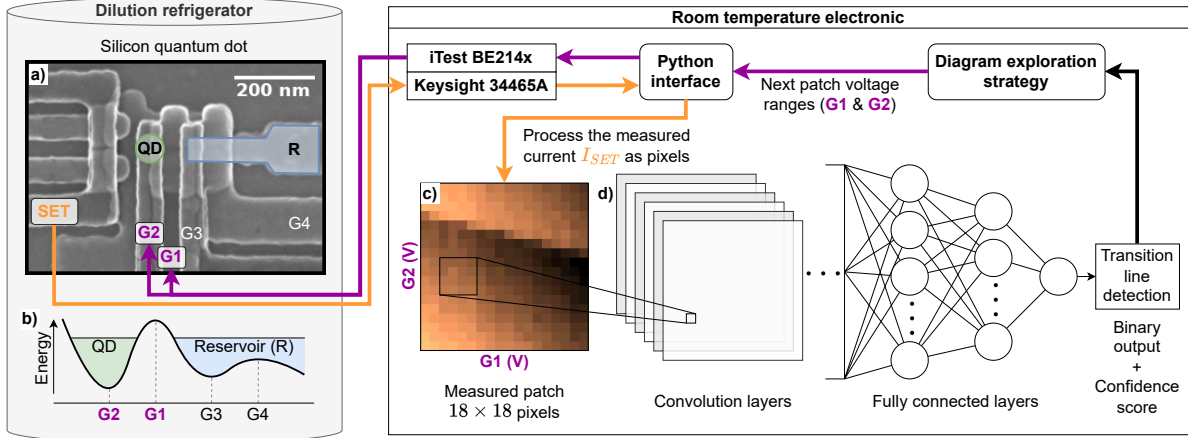


Figure 1: Schematic representation of the experimental setup. A silicon quantum dot (QD) device is cooled in a dilution refrigerator with a base temperature of 20 mK. The voltages at gates 3 (G3) and 4 (G4) are fixed, while a *iTest BE214x* controls the voltages at gates 1 (G1) and 2 (G2) through a Python interface. The scan coordinates are defined by an autonomous closed-loop procedure using a trained convolutional neural network (CNN) and an exploration strategy algorithm. **a)** Scanning electron microscope (SEM) image of a silicon QD device with overlapping gates, similar to the one used during this experiment. The electrons flow from the reservoir (R) to the QD. See [66] for fabrication details. **b)** Energy diagram representing the formation of a single QD in this device. **c)** A subsection of the voltage space (referred to as “patch”) was scanned by sweeping the voltages at gates G1 and G2 and measuring the current using the single-electron transistor (SET) connected to a *Keysight 34465A* multimeter. **d)** Trained CNN that processed the measured patch through two convolutional layers and two fully connected layers to infer the presence of a transition line as a binary output.

The autotuning is approached as an exploration problem, where we start from a random unknown position in the voltage space, gather information about the surroundings by performing local measurements, and search for the targeted charge regime. The transition lines guide the exploration by providing valuable information regarding the number of electrons in the QD. One exploration step consists of scanning a subsection of the voltage space (referred to as “patch” and represented in Figure 1c), sending it to the input of a CNN-based line detection model and deciding the next area to explore based on an exploration strategy (see Figure 2). The patch size is fixed to 18×18 data points as a tradeoff between the measurement time (a smaller area is faster to scan) and the line detection accuracy (a larger area simplifies the line detection). Due to the noisy nature of the measurements and the small size of the patch, classical signal processing and pattern detection methods [67–70] are not robust enough to reliably detect transition lines [35, 48, 49, 53]. We opted for a supervised classification approach using a deep neural network (DNN) [71], which is known to be the best-performing method for pattern detection in noisy images [62–64, 72, 73].

The line detection and exploration strategy are based on the autotuning method described in detail by Yon et al. [51] (see Supplementary Section S4). Nine stability diagrams, measured during previous experiments on similar QD devices and manually annotated, are used to generate a training set of 33,429 patches. Each of these patches is categorized as “line” or “no-line” depending on whether an annotation of a transition line intersects its center. More information on the diagram annotation and patch labeling is available in Supplementary Section S1. A CNN (represented in Figure 1d) is then optimized using gradient backpropagation [74] to classify patches in the training set (refer to Supplementary Section S2 for details on the training methodology).

The trained CNN is transferred to a computer connected to a *iTest BE214x* that is capable of controlling the voltage applied to each gate of the QD device and measuring the SET current using a *Keysight 34465A* multimeter, as illustrated in Figure 1. The autotuning algorithm, implemented in Python², plays a central role at each step of the exploration by: (i) determining the next patch to measure based on the exploration strategy, (ii) transferring the voltage sweeping instructions to the multimeter, (iii) processing the measured current as a normalized image, and (iv) detecting a transition line by feeding the measured patch to the CNN input. To reduce the risk of tuning failures induced by potential patch misclassifications, each inference is associated with a confidence score that estimates the model’s uncertainty for a given input. This score is calculated using a simple distance-based heuristic [75, 76] (more information in Supplementary Section S3). When a patch is classified with a confidence score under the threshold, a verification procedure is

²Python source code: github.com/3it-inpaqt/dot-calibration-v2

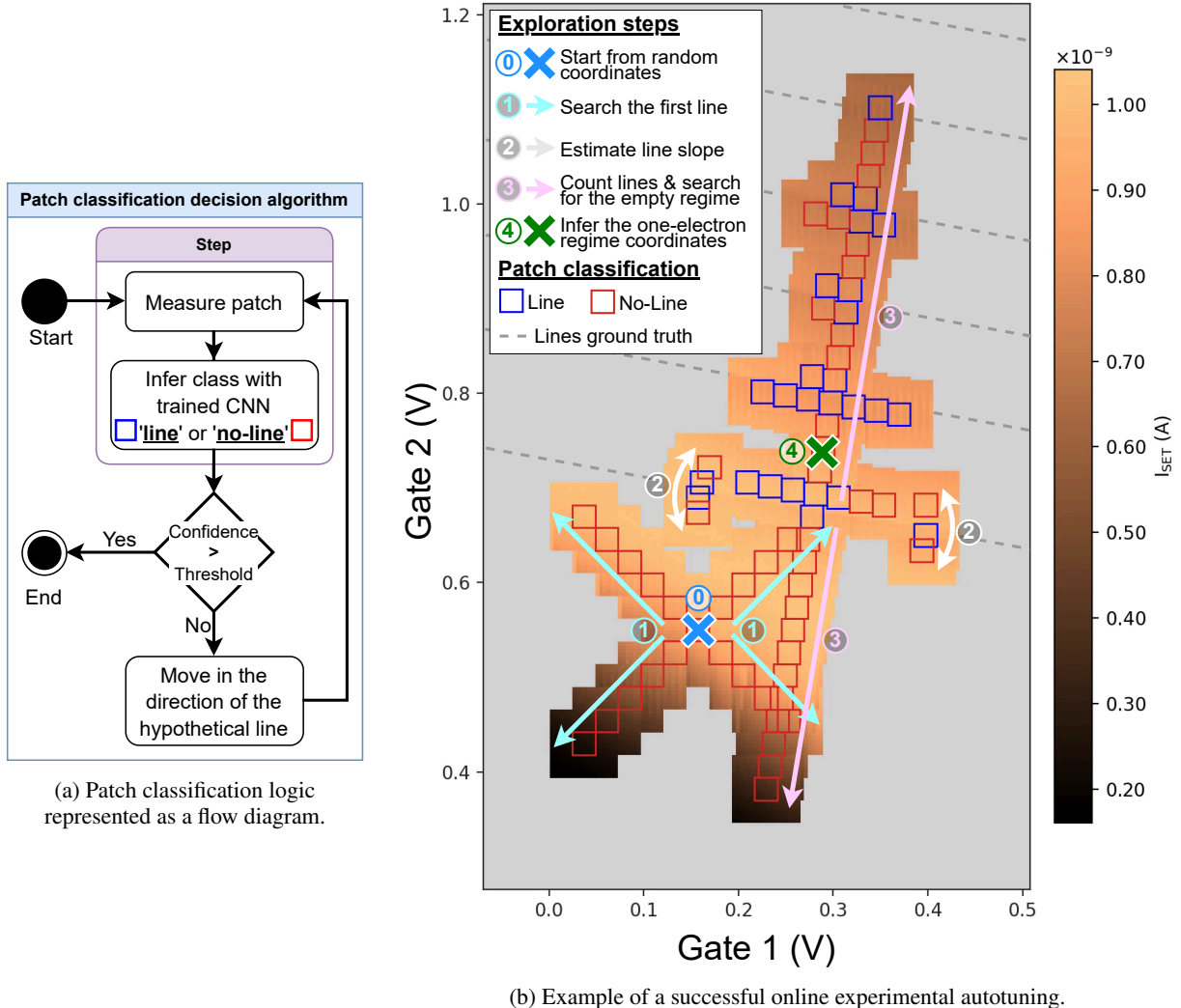


Figure 2: Autonomous exploration strategy. One patch classification step of the algorithm is described in the subfigure (a). Multiple iterations of this step are represented by the blue and red squares in the subfigure (b). In which, the arrows represent the direction of the exploration, and the gray area represents the unmeasured voltage space for this run. The cyan arrows (1) represent the exploration in four directions to search for the first transition line. The white arrows (2) represent the slope estimation step, performed by scanning two sections of the first detected line. Finally, the pink arrows (3) perpendicular to the estimated line slope represent the empty regime search (*down*) and the line count (*up*) procedure. A complete scan of this diagram is given in Figure 3a. See Supplementary Section S4 for more detail regarding this autonomous exploration method.

automatically triggered to validate or refute the presence of a line in the surrounding area. This uncertainty-based exploration has been demonstrated to significantly improve the tuning success rate in offline experiments [51]. It is therefore expected to improve the robustness of autotuning in the case of unexpected perturbations related to the experimental context.

A silicon QD device with overlapping gates [66] was installed and cooled down in a dilution refrigerator with a base temperature of 20 mK. Once the device was cooled, we manually configured it in a single-QD state by keeping the voltages of the confinement gates and unused gates at 0 V, while applying 3 V to the gates we wanted to accumulate. These values were determined through standard I–V measurements. We then ran 20 consecutive and independent charge autotuning procedures.

Each run started at a random location (blue crosses in Figure 3b) in a voltage range of $[-0.25 \text{ V}, 0.5 \text{ V}]$ for gate 1 (G1) (working range for the barrier gate between the QD and the reservoir, based on pinch-off measurement) and $[0 \text{ V}, 2 \text{ V}]$ for gate 2 (G2) (working range for a single QD based on I–V characterisations). Defining bounds on the gates’ voltages was necessary to maintain the hardware’s integrity and avoid wasting time on regions incompatible with a single-QD configuration. However, since the boundary values are generally consistent across all samples of the same type, characterization is required only on the first device.

The voltage space was then explored using iterative patch measurements within the starting voltage ranges, extended by a 0.1 V margin in all directions to ensure the exploration did not begin near a boundary. We did not set virtual gates, as the tuning algorithm was designed to adapt to the capacitive crosstalk. At the end of the experimental runs, we performed a complete scan of the explored area. The resulting stability diagram (shown in Figure 3a) was annotated by experts to identify the transition lines and the charge areas (shown in Figure 3c). By placing the final coordinates of the 20 runs in this figure, we were able to count the number of times we reached the targeted one-electron regime.

3 Results

Positioning the final voltage coordinates in a complete scan of the explored stability diagram (Figure 3a) allows us to evaluate which autotuning runs reach the targeted charge regime. Among the 20 experimental tunings performed, 19 (95 %) successfully located the one-electron regime (green crosses in Figure 3b), while only 1 (5 %) autotuning run failed (red cross in Figure 3b). An analysis of this failure revealed that it was not caused by patch misclassification but by a problem in the exploration logic related to the voltage boundaries. This issue has been fixed in the last version of the Python implementation. A visual animation of each run is available in a video³.

Each autotuning run took an average of 2 hours and 9 minutes (standard deviation: 46 min) and 110 steps (standard deviation: 38) to complete. For comparison, scanning the full stability diagram presented in Figure 3a took approximately 7 hours. Each step required 324 current measurements to obtain one patch (for 18×18 pixels), taking an average of 67 seconds using a *Keysight 34465A* multimeter, representing 96 % of the process duration. Thus, data transfer and processing (including the CNN inference time) represent only a fraction of the tuning time. The high variability between run durations is attributable to the variable distance from the random starting point to the one-electron regime. The individual run statistics are available in Supplementary Table S3.

Prior offline benchmarks obtained by applying this autotuning method to similar devices led to a lower tuning success rate (78 %) [51] despite the comparable line detection accuracy of the CNNs. The higher success rate obtained during this online experiment can be explained by several factors: *(i)* Online tuning allows us to precisely select the patch resolution, while offline diagrams need to be interpolated to compensate for the non-homogeneous step size of the voltage sweeping between measurements (see comparison examples in Supplementary Section S6). This data processing is detrimental to the measurement quality and could explain some line detection failures during offline tests. *(ii)* The fixed voltage range covered by offline diagrams often artificially increases the tuning difficulty by allowing for the exploration of irrelevant areas (e.g., beyond the barrier threshold). *(iii)* Offline autotuning experiments were performed on data measured from multiple devices, covering an extensive range of physical defects and measurement noise. The unique device used in this online experiment appears to be of a good quality (e.g., low noise, no parasitic dots), providing optimal autotuning conditions.

4 Discussion

This online experiment demonstrates the feasibility of autonomous real-time tuning based on ML. It validates that the expected distributional shift between the offline training data and the online measurements is not detrimental to the procedure’s performance. On the contrary, the higher success rate observed in this experiment, compared to previous

³Online autotuning experiment video: youtu.be/zGIQWEZex0s

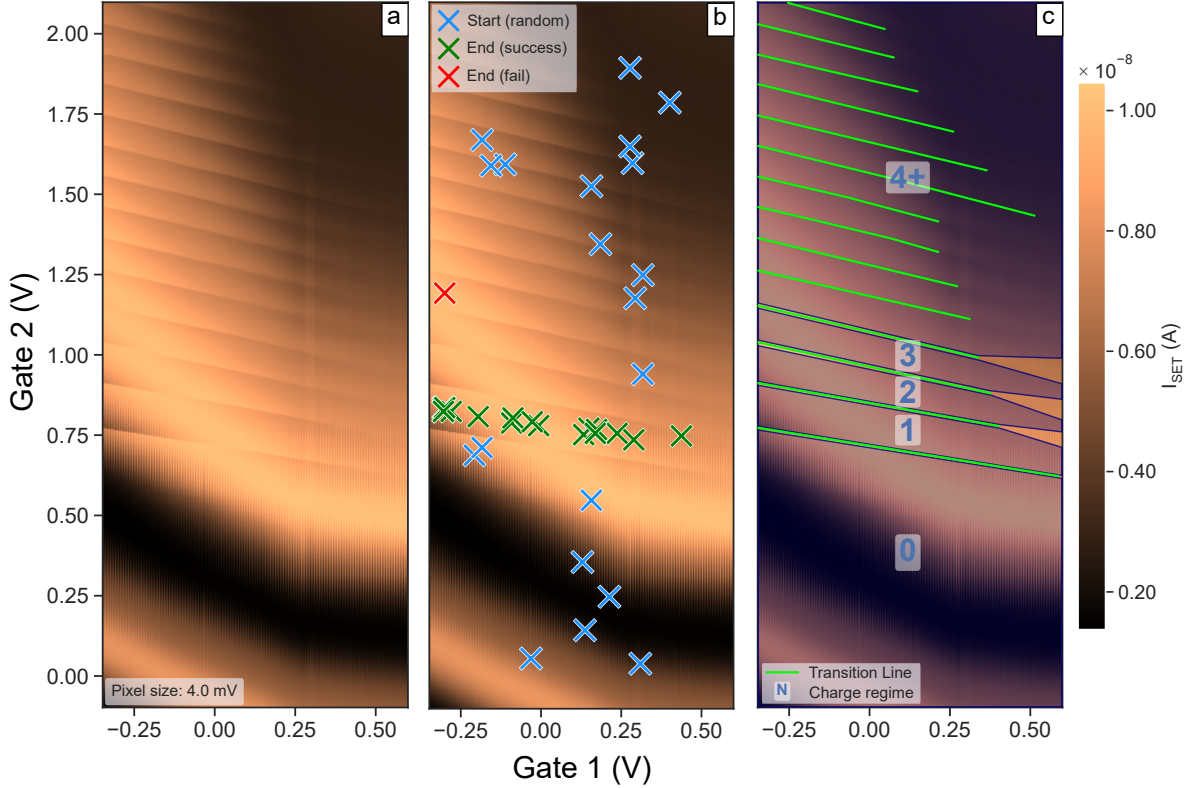


Figure 3: Complete scan of the explored stability diagram, processed after the experiment. **a)** Representation of a stability diagram as an image, where pixel values encode the current measured using the single-electron transistor (SET) as a function of the gate voltages applied to the quantum dot (QD) (see Figure 1). **b)** Start and end coordinates of the 20 online experimental autotuning runs. The blue crosses represent the random starting point of the runs. The green crosses represent the final coordinates of the successful autotuning runs (when the coordinates are inside the area annotated as a one-electron regime). The red cross represents the end coordinates of the run that did not reach the target regime. **c)** Same diagram with manual annotations of transition lines in green and charge regime areas in blue. The region with four or more charges is annotated as “4+”. The voltage areas not covered by a charge annotation (due to fading lines) are considered “*unknown charge regimes*”.

offline benchmarks on similar devices [51], suggests that the absence of preprocessing improved the robustness of the autotuning. We also confirmed that the line detection model and the exploration strategy were versatile enough to successfully tune a QD device that was not in the training set.

The relatively slow tuning time (>2 hours) does not satisfy the requirement for practical tuning of a large QD array. However, the SET measurement time, identified as the main bottleneck, could be drastically improved by optimizing the sensing method and hardware. For example, one could speed up the measurement time by a factor of 10 by implementing the measurement sequence on a dedicated processor [77] (e.g., a field-programmable gate array (FPGA)). This approach would cut the communication time between the instruments and the control computer, allowing for faster sweep rates. The radio-frequency reflectometry technique [33, 78] could also be used to speed up the charge sensing by measuring the impedance of the SET sensor at a fixed frequency, enabling single-shot readouts with only several microseconds of integration time [79]. This time can even be reduced to 400 ns with a Josephson parametric amplifier that also provides a high signal-to-noise ratio [77]. However, the whole measurement pipeline should be optimized to take advantage of this hardware acceleration, including the data transfer, latency, and processing time. On the other hand, it is possible to limit the effect of this measurement bottleneck with a software approach; for example, by optimizing the meta-parameters (Supplementary Tables S1 and S2) in a way that reduces the number of measured points (e.g., smaller patches and a larger voltage distance between pixels) and reducing the number of steps (e.g., higher confidence threshold and smaller voltage boundaries). Finally, improving the fabrication processes of the QD chip is likely to reduce device-to-device variability, which will directly improve the autotuning robustness and reduce the number of steps by narrowing the voltage ranges to explore.

Further optimization can be achieved by moving the control electronics (represented in the right panel of Figure 1) to the cryogenic environment inside the dilution refrigerator. Bringing the control electronics closer to the tuned device, either by co-integrating them with the QD chip [22, 25] or with additional nearby electronics, can reduce the parasitic capacitance added to the current measurements and allow for the control of large-scale arrays of QDs by circumventing the wiring bottleneck [80] between the QD devices and the control electronics. However, this *in situ* autotuning scheme requires the development of cryo-compatible and low-power custom electronics [51, 81–84].

Acknowledgments

V.Y. acknowledges Christian Lupien’s valuable technical assistance in interfacing the experimental hardware with Python.

V.Y., B.G., Y.B., and D.D. acknowledge support from the National Science Engineering Research Council of Canada, Grant ALLRP 580722–22, and the Fonds de Recherche du Québec—Nature et Technologies, Grant 300253.

C.R., J.R., A.M., D.L., and E.D.F acknowledge support from the FRQNT établissement de la relève professorale, Grant 2020–NC–268397, and the CRSNG, Grant RGPIN–2020–0573.

R.G.M. acknowledges support from NSERC and the Perimeter Institute for Theoretical Physics. Research at the Perimeter Institute is supported in part by the Government of Canada through the Department of Innovation, Science and Economic Development Canada and by the Province of Ontario through the Ministry of Economic Development, Job Creation and Trade.

Conflicts of interest

The authors declare no conflicts of interest.

Author contributions

All authors contributed to this article and approved of the submitted version.

Victor Yon: methodology, software implementation, experiments, results analysis and visualization, writing—original draft preparation.

Bastien Galaup: software implementation, experiments, manuscript review.

Claude Rohrbacher, Joffrey Rivard, Alexis Morel, and Dominic Leclerc: initialize and configure the experimental setup, methodology, manuscript review.

Clement Godfrin, Ruoyu Li, Stefan Kubicek, and Kristiaan De Greve: manufactured the devices, manuscript review.

Roger Melko: supervision, manuscript review.

Eva Dupont-Ferrier, Yann Beilliard, and Dominique Drouin: methodology, supervision, funding acquisition, manuscript review, editing.

Code and data availability

The Python source code used to aggregate and build the dataset is publicly accessible on *GitHub*: github.com/3it-inaqt/qdsd-dataset.

The Python source code used to run all the experiments presented in this article is publicly accessible on *GitHub*: github.com/3it-inaqt/dot-calibration-v2.

The raw and processed stability diagram measurements used to train the line detection model for this experiment are publicly available for download from Yon et al. [65]. The subset used to train the models in this paper is referred to as silicon overlapping gates quantum dot (Si-OG-QD).

All trained models, experimental measurements, and results presented in this article are publicly available for download from Yon et al. [85].

References

- [1] Daniel Loss and David P. DiVincenzo. Quantum computation with quantum dots. *Physical Review A*, 57(1): 120–126, January 1998. ISSN 1094-1622. doi:10.1103/physreva.57.120. URL <http://doi.org/10.1103/PhysRevA.57.120>.
- [2] M. Veldhorst, C. H. Yang, J. C. C. Hwang, W. Huang, J. P. Dehollain, J. T. Muhonen, S. Simmons, A. Laucht, F. E. Hudson, K. M. Itoh, A. Morello, and A. S. Dzurak. A two-qubit logic gate in silicon. *Nature*, 526(7573):410–414, October 2015. ISSN 1476-4687. doi:10.1038/nature15263. URL <http://doi.org/10.1038/nature15263>.
- [3] T. F. Watson, S. G. J. Philips, E. Kawakami, D. R. Ward, P. Scarlino, M. Veldhorst, D. E. Savage, M. G. Lagally, Mark Friesen, S. N. Coppersmith, M. A. Eriksson, and L. M. K. Vandersypen. A programmable two-qubit quantum processor in silicon. *Nature*, 555(7698):633–637, February 2018. ISSN 1476-4687. doi:10.1038/nature25766. URL <http://doi.org/10.1038/nature25766>.
- [4] Guido Burkard, Thaddeus D. Ladd, Andrew Pan, John M. Nichol, and Jason R. Petta. Semiconductor spin qubits. *Reviews of Modern Physics*, 95(2), June 2023. ISSN 1539-0756. doi:10.1103/revmodphys.95.025003. URL <http://doi.org/10.1103/RevModPhys.95.025003>.
- [5] Floris A. Zwanenburg, Andrew S. Dzurak, Andrea Morello, Michelle Y. Simmons, Lloyd C. L. Hollenberg, Gerhard Klimeck, Sven Rogge, Susan N. Coppersmith, and Mark A. Eriksson. Silicon quantum electronics. *Reviews of Modern Physics*, 85(3):961–1019, July 2013. ISSN 1539-0756. doi:10.1103/revmodphys.85.961. URL <http://doi.org/10.1103/RevModPhys.85.961>.
- [6] Kenta Takeda, Jun Kamioka, Tomohiro Otsuka, Jun Yoneda, Takashi Nakajima, Matthieu R. Delbecq, Shinichi Amaha, Giles Allison, Tetsuo Kodera, Shunri Oda, and Seigo Tarucha. A fault-tolerant addressable spin qubit in a natural silicon quantum dot. *Science Advances*, 2(8), August 2016. ISSN 2375-2548. doi:10.1126/sciadv.1600694. URL <http://doi.org/10.1126/sciadv.1600694>.
- [7] Jun Yoneda, Kenta Takeda, Tomohiro Otsuka, Takashi Nakajima, Matthieu R. Delbecq, Giles Allison, Takumu Honda, Tetsuo Kodera, Shunri Oda, Yusuke Hoshi, Noritaka Usami, Kohei M. Itoh, and Seigo Tarucha. A quantum-dot spin qubit with coherence limited by charge noise and fidelity higher than 99.9%. *Nature Nanotechnology*, 13(2):102–106, December 2017. ISSN 1748-3395. doi:10.1038/s41565-017-0014-x. URL <http://doi.org/10.1038/s41565-017-0014-x>.
- [8] Adam R. Mills, Charles R. Guinn, Michael J. Gullans, Anthony J. Sigillito, Mayer M. Feldman, Erik Nielsen, and Jason R. Petta. Two-qubit silicon quantum processor with operation fidelity exceeding 99%. *Science Advances*, 8(14), April 2022. ISSN 2375-2548. doi:10.1126/sciadv.abn5130. URL <http://doi.org/10.1126/sciadv.abn5130>.
- [9] Akito Noiri, Kenta Takeda, Takashi Nakajima, Takashi Kobayashi, Amir Sammak, Giordano Scappucci, and Seigo Tarucha. A shuttling-based two-qubit logic gate for linking distant silicon quantum processors. *Nature Communications*, 13(1), September 2022. ISSN 2041-1723. doi:10.1038/s41467-022-33453-z. URL <http://doi.org/10.1038/s41467-022-33453-z>.
- [10] Xiao Xue, Maximilian Russ, Nodar Samkharadze, Brennan Undseth, Amir Sammak, Giordano Scappucci, and Lieven M. K. Vandersypen. Quantum logic with spin qubits crossing the surface code threshold. *Nature*, 601(7893):343–347, January 2022. ISSN 1476-4687. doi:10.1038/s41586-021-04273-w. URL <http://doi.org/10.1038/s41586-021-04273-w>.
- [11] Aaron J. Weinstein, Matthew D. Reed, Aaron M. Jones, Reed W. Andrews, David Barnes, Jacob Z. Blumoff, Larken E. Euliss, Kevin Eng, Bryan H. Fong, Sieu D. Ha, Daniel R. Hulbert, Clayton A. C. Jackson, Michael Jura, Tyler E. Keating, Joseph Kerckhoff, Andrey A. Kiselev, Justine Matten, Golam Sabbir, Aaron Smith, Jeffrey Wright, Matthew T. Rakher, Thaddeus D. Ladd, and Matthew G. Borselli. Universal logic with encoded spin qubits in silicon. *Nature*, 615(7954):817–822, February 2023. ISSN 1476-4687. doi:10.1038/s41586-023-05777-3. URL <http://doi.org/10.1038/s41586-023-05777-3>.
- [12] Will Gilbert, Tuomo Tantt, Wee Han Lim, MengKe Feng, Jonathan Y. Huang, Jesus D. Cifuentes, Santiago Serrano, Philip Y. Mai, Ross C. C. Leon, Christopher C. Escott, Kohei M. Itoh, Nikolay V. Abrosimov, Hans-Joachim Pohl, Michael L. W. Thewalt, Fay E. Hudson, Andrea Morello, Arne Laucht, Chih Hwan Yang, Andre Saraiva, and Andrew S. Dzurak. On-demand electrical control of spin qubits. *Nature Nanotechnology*, 18(2): 131–136, January 2023. ISSN 1748-3395. doi:10.1038/s41565-022-01280-4. URL <http://doi.org/10.1038/s41565-022-01280-4>.
- [13] Alexei M. Tyryshkin, Shinichi Tojo, John J. L. Morton, Helge Riemann, Nikolai V. Abrosimov, Peter Becker, Hans-Joachim Pohl, Thomas Schenkel, Michael L. W. Thewalt, Kohei M. Itoh, and S. A. Lyon. Electron spin coherence exceeding seconds in high-purity silicon. *Nature Materials*, 11(2):143–147, December 2011. ISSN 1476-4660. doi:10.1038/nmat3182. URL <http://doi.org/10.1038/nmat3182>.

- [14] M. Veldhorst, J. C. C. Hwang, C. H. Yang, A. W. Leenstra, B. de Ronde, J. P. Dehollain, J. T. Muhonen, F. E. Hudson, K. M. Itoh, A. Morello, and A. S. Dzurak. An addressable quantum dot qubit with fault-tolerant control-fidelity. *Nature Nanotechnology*, 9(12):981–985, October 2014. ISSN 1748-3395. doi:10.1038/nnano.2014.216. URL <http://doi.org/10.1038/nnano.2014.216>.
- [15] Luca Petit, Maximilian Russ, Gertjan H. G. J. Eenink, William I. L. Lawrie, James S. Clarke, Lieven M. K. Vandersypen, and Menno Veldhorst. Design and integration of single-qubit rotations and two-qubit gates in silicon above one kelvin. *Communications Materials*, 3(1), November 2022. ISSN 2662-4443. doi:10.1038/s43246-022-00304-9. URL <http://doi.org/10.1038/s43246-022-00304-9>.
- [16] C. H. Yang, R. C. C. Leon, J. C. C. Hwang, A. Saraiva, T. Tanttu, W. Huang, J. Camirand Lemyre, K. W. Chan, K. Y. Tan, F. E. Hudson, K. M. Itoh, A. Morello, M. Pioro-Ladrière, A. Laucht, and A. S. Dzurak. Operation of a silicon quantum processor unit cell above one kelvin. *Nature*, 580(7803):350–354, April 2020. ISSN 1476-4687. doi:10.1038/s41586-020-2171-6. URL <http://doi.org/10.1038/s41586-020-2171-6>.
- [17] Jonathan Y. Huang, Rocky Y. Su, Wee Han Lim, MengKe Feng, Barnaby van Straaten, Brandon Severin, Will Gilbert, Nard Dumoulin Stuyck, Tuomo Tanttu, Santiago Serrano, Jesus D. Cifuentes, Ingvild Hansen, Amanda E. Seedhouse, Ensar Vahapoglu, Ross C. C. Leon, Nikolay V. Abrosimov, Hans-Joachim Pohl, Michael L. W. Thewalt, Fay E. Hudson, Christopher C. Escott, Natalia Ares, Stephen D. Bartlett, Andrea Morello, Andre Saraiva, Arne Laucht, et al. High-fidelity spin qubit operation and algorithmic initialization above 1 k. *Nature*, 627(8005):772–777, March 2024. ISSN 1476-4687. doi:10.1038/s41586-024-07160-2. URL <http://doi.org/10.1038/s41586-024-07160-2>.
- [18] R. Maurand, X. Jehl, D. Kotekar-Patil, A. Corna, H. Bohuslavskiy, R. Laviéville, L. Hutin, S. Barraud, M. Vinet, M. Sanquer, and S. De Franceschi. A cmos silicon spin qubit. *Nature Communications*, 7(1), November 2016. ISSN 2041-1723. doi:10.1038/ncomms13575. URL <http://doi.org/10.1038/ncomms13575>.
- [19] N. I. Dumoulin Stuyck, R. Li, C. Godfrin, A. Elsayed, S. Kubicek, J. Jussot, B. T. Chan, F. A. Mohiyaddin, M. Shehata, G. Simion, Y. Canvel, L. Goux, M. Heyns, B. Govoreanu, and I. P. Radu. Uniform spin qubit devices with tunable coupling in an all-silicon 300 mm integrated process. In *2021 Symposium on VLSI Circuits*, page 1–2. Ieee, June 2021. doi:10.23919/vlsicircuits52068.2021.9492427. URL <http://doi.org/10.23919/VLSICircuits52068.2021.9492427>.
- [20] A. M. J. Zwerver, T. Krähenmann, T. F. Watson, L. Lampert, H. C. George, R. Pillarisetty, S. A. Bojarski, P. Amin, S. V. Amitonov, J. M. Boter, R. Caudillo, D. Correas-Serrano, J. P. Dehollain, G. Droulers, E. M. Henry, R. Kotlyar, M. Lodari, F. Lüthi, D. J. Michalak, B. K. Mueller, S. Neyens, J. Roberts, N. Samkharadze, G. Zheng, O. K. Zietz, et al. Qubits made by advanced semiconductor manufacturing. *Nature Electronics*, 5(3):184–190, March 2022. ISSN 2520-1131. doi:10.1038/s41928-022-00727-9. URL <http://doi.org/10.1038/s41928-022-00727-9>.
- [21] S. Rochette, M. Rudolph, A.-M. Roy, M. J. Curry, G. A. Ten Eyck, R. P. Manginell, J. R. Wendt, T. Pluym, S. M. Carr, D. R. Ward, M. P. Lilly, M. S. Carroll, and M. Pioro-Ladrière. Quantum dots with split enhancement gate tunnel barrier control. *Applied Physics Letters*, 114(8), February 2019. ISSN 1077-3118. doi:10.1063/1.5091111. URL <http://doi.org/10.1063/1.5091111>.
- [22] C. Rohrbacher, J. Rivard, R. Ritzenthaler, B. Bureau, C. Lupien, H. Mertens, N. Horiguchi, and E. Dupont-Ferrier. Dual operation of gate-all-around silicon nanowires at cryogenic temperatures: Fet and quantum dot. *ArXiv*, 2023. doi:10.48550/arxiv.2312.00903. URL <https://arxiv.org/abs/2312.00903>. Preprint.
- [23] M. F. Gonzalez-Zalba, S. de Franceschi, E. Charbon, T. Meunier, M. Vinet, and A. S. Dzurak. Scaling silicon-based quantum computing using cmos technology. *Nature Electronics*, 4(12):872–884, December 2021. ISSN 2520-1131. doi:10.1038/s41928-021-00681-y. URL <http://doi.org/10.1038/s41928-021-00681-y>.
- [24] Samuel Neyens, Otto K. Zietz, Thomas F. Watson, Florian Luthi, Aditi Nethewala, Hubert C. George, Eric Henry, Mohammad Islam, Andrew J. Wagner, Felix Borjans, Elliot J. Connors, J. Corrigan, Matthew J. Curry, Daniel Keith, Roza Kotlyar, Lester F. Lampert, Mateusz T. Mądzik, Kent Millard, Fahd A. Mohiyaddin, Stefano Pellerano, Ravi Pillarisetty, Mick Ramsey, Rostyslav Savvitsky, Simon Schaal, Guoji Zheng, et al. Probing single electrons across 300-mm spin qubit wafers. *Nature*, 629(8010):80–85, May 2024. ISSN 1476-4687. doi:10.1038/s41586-024-07275-6. URL <http://doi.org/10.1038/s41586-024-07275-6>.
- [25] Claude Rohrbacher, Dominic Leclerc, Joffrey Rivard, Romain Ritzenthaler, Christian Lupien, Hans Mertens, Naoto Horiguchi, and Eva Dupont-Ferrier. Nanosheet transistors produced in 300 mm fabrication platform for quantum computing. 2024. To be published.
- [26] J P Dodson, Nathan Holman, Brandur Thorgrimsson, Samuel F Neyens, E R MacQuarrie, Thomas McJunkin, Ryan H Foote, L F Edge, S N Coppersmith, and M A Eriksson. Fabrication process and failure analysis for robust quantum dots in silicon. *Nanotechnology*, 31(50):505001, October 2020. ISSN 1361-6528. doi:10.1088/1361-6528/abb559. URL <http://doi.org/10.1088/1361-6528/abb559>.

- [27] Charles Tahan. Opinion: Democratizing spin qubits. *Quantum*, 5:584, November 2021. ISSN 2521-327x. doi:10.22331/q-2021-11-18-584. URL <http://doi.org/10.22331/q-2021-11-18-584>.
- [28] J. Michniewicz and M. S. Kim. Leveraging off-the-shelf silicon chips for quantum computing. *Applied Physics Letters*, 124(26), June 2024. ISSN 1077-3118. doi:10.1063/5.0207162. URL <http://doi.org/10.1063/5.0207162>.
- [29] Andre Saraiva, Wee Han Lim, Chih Hwan Yang, Christopher C. Escott, Arne Laucht, and Andrew S. Dzurak. Materials for silicon quantum dots and their impact on electron spin qubits. *Advanced Functional Materials*, 32(3), December 2021. ISSN 1616-3028. doi:10.1002/adfm.202105488. URL <http://doi.org/10.1002/adfm.202105488>.
- [30] Francesco Borsoi, Nico W. Hendrickx, Valentin John, Marcel Meyer, Sayr Motz, Floor van Riggelen, Amir Sammak, Sander L. de Snoo, Giordano Scappucci, and Menno Veldhorst. Shared control of a 16 semiconductor quantum dot crossbar array. *Nature Nanotechnology*, 19(1):21–27, August 2023. ISSN 1748-3395. doi:10.1038/s41565-023-01491-3. URL <http://doi.org/10.1038/s41565-023-01491-3>.
- [31] Pierre-Antoine Mouny, Raphaël Dawant, Patrick Dufour, Matthieu Valdenaire, Serge Ecoffey, Michel Pioro-Ladrière, Yann Beillard, and Dominique Drouin. Towards scalable cryogenic quantum dot biasing using memristor-based dc sources. *ArXiv*, 2024. doi:10.48550/arxiv.2404.10694. URL <https://arxiv.org/abs/2404.10694>. Preprint.
- [32] Justyna P. Zwolak and Jacob M. Taylor. Colloquium : Advances in automation of quantum dot devices control. *Reviews of Modern Physics*, 95(1), February 2023. ISSN 1539-0756. doi:10.1103/revmodphys.95.011006. URL <http://doi.org/10.1103/RevModPhys.95.011006>.
- [33] Anton Zubchenko, Danielle Middlebrooks, Torbjørn Rasmussen, Lara Lausen, Ferdinand Kuemmeth, Anasua Chatterjee, and Justyna P. Zwolak. Autonomous bootstrapping of quantum dot devices. *ArXiv*, 2024. doi:10.48550/arxiv.2407.20061. URL <https://arxiv.org/abs/2407.20061>. Preprint.
- [34] Tyler J. Kovach, Daniel Schug, M. A. Wolfe, E. R. MacQuarrie, Patrick J. Walsh, Jared Benson, Mark Friesen, M. A. Eriksson, and Justyna P. Zwolak. Batis: Bootstrapping, autonomous testing, and initialization system for quantum dot devices, 2024. URL <https://arxiv.org/abs/2412.07676>.
- [35] Joshua Ziegler, Florian Luthi, Mick Ramsey, Felix Borjans, Guoji Zheng, and Justyna P. Zwolak. Tuning arrays with rays: Physics-informed tuning of quantum dot charge states. *Physical Review Applied*, 20(3), September 2023. ISSN 2331-7019. doi:10.1103/physrevapplied.20.034067. URL <http://doi.org/10.1103/PhysRevApplied.20.034067>.
- [36] Hanwei Liu, Baochuan Wang, Ning Wang, Zhonghai Sun, Huili Yin, Haiou Li, Gang Cao, and Guoping Guo. An automated approach for consecutive tuning of quantum dot arrays. *Applied Physics Letters*, 121(8), August 2022. ISSN 1077-3118. doi:10.1063/5.0111128. URL <http://doi.org/10.1063/5.0111128>.
- [37] Justyna P. Zwolak, Thomas McJunkin, Sandesh S. Kalantre, J.P. Dodson, E.R. MacQuarrie, D.E. Savage, M.G. Lagally, S.N. Coppersmith, Mark A. Eriksson, and Jacob M. Taylor. Autotuning of double-dot devices in situ with machine learning. *Physical Review Applied*, 13(3), March 2020. ISSN 2331-7019. doi:10.1103/physrevapplied.13.034075. URL <http://doi.org/10.1103/PhysRevApplied.13.034075>.
- [38] Sandesh S. Kalantre, Justyna P. Zwolak, Stephen Ragole, Xingyao Wu, Neil M. Zimmerman, M. D. Stewart, and Jacob M. Taylor. Machine learning techniques for state recognition and auto-tuning in quantum dots. *npj Quantum Information*, 5(1), January 2019. ISSN 2056-6387. doi:10.1038/s41534-018-0118-7. URL <http://doi.org/10.1038/s41534-018-0118-7>.
- [39] J Darulová, M Troyer, and M C Cassidy. Evaluation of synthetic and experimental training data in supervised machine learning applied to charge-state detection of quantum dots. *Machine Learning: Science and Technology*, 2(4):045023, September 2021. ISSN 2632-2153. doi:10.1088/2632-2153/ac104c. URL <http://doi.org/10.1088/2632-2153/ac104c>.
- [40] H. Moon, D. T. Lennon, J. Kirkpatrick, N. M. van Esbroeck, L. C. Camenzind, Liuqi Yu, F. Vigneau, D. M. Zumbühl, G. A. D. Briggs, M. A. Osborne, D. Sejdinovic, E. A. Laird, and N. Ares. Machine learning enables completely automatic tuning of a quantum device faster than human experts. *Nature Communications*, 11(1), August 2020. ISSN 2041-1723. doi:10.1038/s41467-020-17835-9. URL <http://doi.org/10.1038/s41467-020-17835-9>.
- [41] Joshua Ziegler, Thomas McJunkin, E.S. Joseph, Sandesh S. Kalantre, Benjamin Harpt, D.E. Savage, M.G. Lagally, M.A. Eriksson, Jacob M. Taylor, and Justyna P. Zwolak. Toward robust autotuning of noisy quantum dot devices. *Physical Review Applied*, 17(2), February 2022. ISSN 2331-7019. doi:10.1103/physrevapplied.17.024069. URL <http://doi.org/10.1103/PhysRevApplied.17.024069>.

- [42] B. Severin, D. T. Lennon, L. C. Camenzind, F. Vigneau, F. Fedele, D. Jirovec, A. Ballabio, D. Chrastina, G. Isella, M. de Kruijf, M. J. Carballido, S. Svab, A. V. Kuhlmann, S. Geyer, F. N. M. Froning, H. Moon, M. A. Osborne, D. Sejdinovic, G. Katsaros, D. M. Zumbühl, G. A. D. Briggs, and N. Ares. Cross-architecture tuning of silicon and sige-based quantum devices using machine learning. *Scientific Reports*, 14(1), July 2024. ISSN 2045-2322. doi:10.1038/s41598-024-67787-z. URL <http://doi.org/10.1038/s41598-024-67787-z>.
- [43] Justin K Perron, M D Stewart Jr, and Neil M Zimmerman. A quantitative study of bias triangles presented in chemical potential space. *Journal of Physics: Condensed Matter*, 27(23):235302, May 2015. ISSN 1361-648x. doi:10.1088/0953-8984/27/23/235302. URL <http://doi.org/10.1088/0953-8984/27/23/235302>.
- [44] Toivo Hensgens. *Emulating Fermi-Hubbard physics with quantum dots*. Phd thesis, Delft University of Technology, 2018. URL <http://resolver.tudelft.nl/uuid:b71f3b0b-73a0-4996-896c-84ed43e72035>.
- [45] T.-K. Hsiao, C.J. van Diepen, U. Mukhopadhyay, C. Reichl, W. Wegscheider, and L.M.K. Vandersypen. Efficient orthogonal control of tunnel couplings in a quantum dot array. *Physical Review Applied*, 13(5), May 2020. ISSN 2331-7019. doi:10.1103/physrevapplied.13.054018. URL <http://doi.org/10.1103/PhysRevApplied.13.054018>.
- [46] C. J. van Diepen, P. T. Eendebak, B. T. Buijtdorp, U. Mukhopadhyay, T. Fujita, C. Reichl, W. Wegscheider, and L. M. K. Vandersypen. Automated tuning of inter-dot tunnel coupling in double quantum dots. *Applied Physics Letters*, 113(3), July 2018. ISSN 1077-3118. doi:10.1063/1.5031034. URL <http://doi.org/10.1063/1.5031034>.
- [47] Anantha S. Rao, Donovan Buterakos, Barnaby van Straaten, Valentin John, Cécile X. Yu, Stefan D. Oosterhout, Lucas Stehouwer, Giordano Scappucci, Menno Veldhorst, Francesco Borsoi, and Justyna P. Zwolak. Mavis: Modular autonomous virtualization system for two-dimensional semiconductor quantum dot arrays, 2024. URL <https://arxiv.org/abs/2411.12516>.
- [48] Stefanie Czischek, Victor Yon, Marc-Antoine Genest, Marc-Antoine Roux, Sophie Rochette, Julien Camirand Lemyre, Mathieu Moras, Michel Pioro-Ladrière, Dominique Drouin, Yann Beilliard, and Roger G Melko. Miniaturizing neural networks for charge state autotuning in quantum dots. *Machine Learning: Science and Technology*, 3(1):015001, November 2021. ISSN 2632-2153. doi:10.1088/2632-2153/ac34db. URL <http://doi.org/10.1088/2632-2153/ac34db>.
- [49] M. Lapointe-Major, O. Germain, J. Camirand Lemyre, D. Lachance-Quirion, S. Rochette, F. Camirand Lemyre, and M. Pioro-Ladrière. Algorithm for automated tuning of a quantum dot into the single-electron regime. *Physical Review B*, 102(8), August 2020. ISSN 2469-9969. doi:10.1103/physrevb.102.085301. URL <http://doi.org/10.1103/PhysRevB.102.085301>.
- [50] R. Durrer, B. Kratochwil, J.V. Koski, A.J. Landig, C. Reichl, W. Wegscheider, T. Ihn, and E. Grepova. Automated tuning of double quantum dots into specific charge states using neural networks. *Physical Review Applied*, 13(5), May 2020. ISSN 2331-7019. doi:10.1103/physrevapplied.13.054019. URL <http://doi.org/10.1103/PhysRevApplied.13.054019>.
- [51] Victor Yon, Bastien Galaup, Claude Rohrbacher, Joffrey Rivard, Clément Godfrin, Ruoyu Li, Stefan Kubicek, Kristiaan De Greve, Louis Gaudreau, Eva Dupont-Ferrier, Yann Beilliard, Roger G Melko, and Dominique Drouin. Robust quantum dots charge autotuning using neural network uncertainty. *Machine Learning: Science and Technology*, 5(4):045034, November 2024. ISSN 2632-2153. doi:10.1088/2632-2153/ad88d5. URL <http://doi.org/10.1088/2632-2153/ad88d5>.
- [52] Yui Muto, Takumi Nakaso, Motoya Shinozaki, Takumi Aizawa, Takahito Kitada, Takashi Nakajima, Matthieu R. Delbecq, Jun Yoneda, Kenta Takeda, Akito Noiri, Arne Ludwig, Andreas D. Wieck, Seigo Tarucha, Atsunori Kanemura, Motoki Shiga, and Tomohiro Otsuka. Visual explanations of machine learning model estimating charge states in quantum dots. *APL Machine Learning*, 2(2), April 2024. ISSN 2770-9019. doi:10.1063/5.0193621. URL <http://doi.org/10.1063/5.0193621>.
- [53] T. A. Baart, P. T. Eendebak, C. Reichl, W. Wegscheider, and L. M. K. Vandersypen. Computer-automated tuning of semiconductor double quantum dots into the single-electron regime. *Applied Physics Letters*, 108(21), May 2016. ISSN 1077-3118. doi:10.1063/1.4952624. URL <http://doi.org/10.1063/1.4952624>.
- [54] Marcel Meyer, Corentin Déprez, Ilja N. Meijer, Florian K. Unseld, Saurabh Karwal, Amir Sammak, Giordano Scappucci, Lieven M. K. Vandersypen, and Menno Veldhorst. Single-electron occupation in quantum dot arrays at selectable plunger gate voltage. *Nano Letters*, 23(24):11593–11600, December 2023. ISSN 1530-6992. doi:10.1021/acs.nanolett.3c03349. URL <http://doi.org/10.1021/acs.nanolett.3c03349>.
- [55] Julian D. Teske, Simon Sebastian Humpohl, René Otten, Patrick Bethke, Pascal Cerfontaine, Jonas Dedden, Arne Ludwig, Andreas D. Wieck, and Hendrik Bluhm. A machine learning approach for automated fine-tuning of

- semiconductor spin qubits. *Applied Physics Letters*, 114(13), April 2019. ISSN 1077-3118. doi:10.1063/1.5088412. URL <http://doi.org/10.1063/1.5088412>.
- [56] Tim Botzern, Michael D. Shulman, Sandra Foletti, Shannon P. Harvey, Oliver E. Dial, Patrick Bethke, Pascal Cerfontaine, Robert P. G. McNeil, Diana Mahalu, Vladimir Umansky, Arne Ludwig, Andreas Wieck, Dieter Schuh, Dominique Bougeard, Amir Yacoby, and Hendrik Bluhm. Tuning methods for semiconductor spin qubits. *Physical Review Applied*, 10(5), November 2018. ISSN 2331-7019. doi:10.1103/physrevapplied.10.054026. URL <http://doi.org/10.1103/PhysRevApplied.10.054026>.
- [57] Sahar Daraeizadeh, Shavindra P. Premaratne, and A. Y. Matsuura. Designing high-fidelity multi-qubit gates for semiconductor quantum dots through deep reinforcement learning. In *2020 IEEE International Conference on Quantum Computing and Engineering (QCE)*, page 30–36. IEEE, October 2020. doi:10.1109/qce49297.2020.00014. URL <http://doi.org/10.1109/QCE49297.2020.00014>.
- [58] Jakob Gawlikowski, Cedrique Rovile Njieu-teu Tassi, Mohsin Ali, Jongseok Lee, Matthias Humt, Jianxiang Feng, Anna Kruspe, Rudolph Triebel, Peter Jung, Ribana Roscher, Muhammad Shahzad, Wen Yang, Richard Bamler, and Xiao Xiang Zhu. A survey of uncertainty in deep neural networks. *ArXiv*, 2021. doi:10.48550/arxiv.2107.03342. URL <https://arxiv.org/abs/2107.03342>. Preprint.
- [59] Ian J. Goodfellow, Jonathon Shlens, and Christian Szegedy. Explaining and harnessing adversarial examples. *ArXiv*, 2014. doi:10.48550/arxiv.1412.6572. URL <https://arxiv.org/abs/1412.6572>. Preprint.
- [60] R. Mehrotra, K.R. Namuduri, and N. Ranganathan. Gabor filter-based edge detection. *Pattern Recognition*, 25(12):1479–1494, December 1992. ISSN 0031-3203. doi:10.1016/0031-3203(92)90121-x. URL [http://doi.org/10.1016/0031-3203\(92\)90121-x](http://doi.org/10.1016/0031-3203(92)90121-x).
- [61] Jonas Schuff, Miguel J. Carballido, Madeleine Kotzagiannidis, Juan Carlos Calvo, Marco Caselli, Jacob Rawling, David L. Craig, Barnaby van Straaten, Brandon Severin, Federico Fedele, Simon Svab, Pierre Chevalier Kwon, Rafael S. Egli, Taras Patlatiuk, Nathan Korda, Dominik Zumbühl, and Natalia Ares. Fully autonomous tuning of a spin qubit. *ArXiv*, 2024. doi:10.48550/arxiv.2402.03931. URL <https://arxiv.org/abs/2402.03931>. Preprint.
- [62] Alex Krizhevsky, Ilya Sutskever, and Geoffrey E. Hinton. Imagenet classification with deep convolutional neural networks. *Communications of the ACM*, 60(6):84–90, May 2017. ISSN 1557-7317. doi:10.1145/3065386. URL <http://doi.org/10.1145/3065386>.
- [63] Keiron O’Shea and Ryan Nash. An introduction to convolutional neural networks. *ArXiv*, 2015. doi:10.48550/arxiv.1511.08458. URL <https://arxiv.org/abs/1511.08458>. Preprint.
- [64] Aseem Patil and Milind Rane. *Convolutional Neural Networks: An Overview and Its Applications in Pattern Recognition*, page 21–30. Springer Singapore, October 2020. ISBN 9789811570780. doi:10.1007/978-981-15-7078-0_3. URL http://doi.org/10.1007/978-981-15-7078-0_3.
- [65] Victor Yon, Bastien Galaup, Marc-Antoine Roux, Marc-Antoine Genest, Claude Rohrbacher, Joffrey Rivard, Clément Godfrin, Roy Li, Kristiaan De Greve, Sophie Rochette, Julien Camirand-Lemire, Louis Gaudreau, Michel Pioro-Ladrière, Yann Beilliard, Roger G. Melko, Eva Dupont-Ferrier, and Dominique Drouin. Quantum dots stability diagrams dataset, May 2024. URL <https://doi.org/10.5281/zenodo.11402792>.
- [66] A. Elsayed, M. M. K. Shehata, C. Godfrin, S. Kubicek, S. Massar, Y. Canel, J. Jussot, G. Simion, M. Mongillo, D. Wan, B. Govoreanu, I. P. Radu, R. Li, P. Van Dorpe, and K. De Greve. Low charge noise quantum dots with industrial cmos manufacturing. *npj Quantum Information*, 10(1), July 2024. ISSN 2056-6387. doi:10.1038/s41534-024-00864-3. URL <http://doi.org/10.1038/s41534-024-00864-3>.
- [67] Rui Sun, Tao Lei, Qi Chen, Zexuan Wang, Xiaogang Du, Weiqiang Zhao, and Asoke K. Nandi. Survey of image edge detection. *Frontiers in Signal Processing*, 2, March 2022. ISSN 2673-8198. doi:10.3389/frsip.2022.826967. URL <http://doi.org/10.3389/frsip.2022.826967>.
- [68] Priyanka Mukhopadhyay and Bidyut B. Chaudhuri. A survey of hough transform. *Pattern Recognition*, 48(3):993–1010, March 2015. ISSN 0031-3203. doi:10.1016/j.patcog.2014.08.027. URL <http://doi.org/10.1016/j.patcog.2014.08.027>.
- [69] Lijun Ding and Ardeshtir Goshtasby. On the canny edge detector. *Pattern Recognition*, 34(3):721–725, March 2001. ISSN 0031-3203. doi:10.1016/S0031-3203(00)00023-6. URL [http://doi.org/10.1016/S0031-3203\(00\)00023-6](http://doi.org/10.1016/S0031-3203(00)00023-6).
- [70] Christopher M Bishop. *Pattern recognition and machine learning*. Information Science and Statistics. Springer, 1 edition, August 2006. URL <https://core.ac.uk/download/pdf/44152170.pdf>.
- [71] Yann LeCun, Yoshua Bengio, and Geoffrey Hinton. Deep learning. *Nature*, 521(7553):436–444, May 2015. ISSN 1476-4687. doi:10.1038/nature14539. URL <http://doi.org/10.1038/nature14539>.

- [72] Athanasios Voulodimos, Nikolaos Doulamis, Anastasios Doulamis, and Eftychios Protopapadakis. Deep learning for computer vision: A brief review. *Computational Intelligence and Neuroscience*, 2018:1–13, 2018. ISSN 1687-5273. doi:10.1155/2018/7068349. URL <http://doi.org/10.1155/2018/7068349>.
- [73] Lei Cai, Jingyang Gao, and Di Zhao. A review of the application of deep learning in medical image classification and segmentation. *Annals of Translational Medicine*, 8(11):713–713, June 2020. ISSN 2305-5847. doi:10.21037/atm.2020.02.44. URL <http://doi.org/10.21037/atm.2020.02.44>.
- [74] Raúl Rojas. *The Backpropagation Algorithm*, page 149–182. Springer Berlin Heidelberg, 1996. ISBN 9783642610684. doi:10.1007/978-3-642-61068-4_7. URL http://doi.org/10.1007/978-3-642-61068-4_7.
- [75] Hugo Zaragoza and Florence d’Alché Buc. Confidence measures for neural network classifiers. In *Proceedings of the Seventh Int. Conf. Information Processing and Management of Uncertainty in Knowledge Based Systems*, volume 9. Citeseer, 1998.
- [76] Amit Mandelbaum and Daphna Weinshall. Distance-based confidence score for neural network classifiers. *ArXiv*, 2017. doi:10.48550/arxiv.1709.09844. URL <https://arxiv.org/abs/1709.09844>. Preprint.
- [77] J. Stehlik, Y.-Y. Liu, C.M. Quintana, C. Eichler, T.R. Hartke, and J.R. Petta. Fast charge sensing of a cavity-coupled double quantum dot using a josephson parametric amplifier. *Physical Review Applied*, 4(1), July 2015. ISSN 2331-7019. doi:10.1103/physrevapplied.4.014018. URL <http://doi.org/10.1103/PhysRevApplied.4.014018>.
- [78] Y.-Y. Liu, S.G.J. Philips, L.A. Orona, N. Samkharadze, T. McJunkin, E.R. MacQuarrie, M.A. Eriksson, L.M.K. Vandersypen, and A. Yacoby. Radio-frequency reflectometry in silicon-based quantum dots. *Physical Review Applied*, 16(1), July 2021. ISSN 2331-7019. doi:10.1103/physrevapplied.16.014057. URL <http://doi.org/10.1103/PhysRevApplied.16.014057>.
- [79] D. J. Reilly, C. M. Marcus, M. P. Hanson, and A. C. Gossard. Fast single-charge sensing with a rf quantum point contact. *Applied Physics Letters*, 91(16), October 2007. ISSN 1077-3118. doi:10.1063/1.2794995. URL <http://doi.org/10.1063/1.2794995>.
- [80] D. J. Reilly. Challenges in scaling-up the control interface of a quantum computer. In *2019 IEEE International Electron Devices Meeting (IEDM)*. Ieee, December 2019. doi:10.1109/iedm19573.2019.8993497. URL <http://doi.org/10.1109/IEDM19573.2019.8993497>.
- [81] Pierre-Antoine Mouny, Raphaël Dawant, Bastien Galaup, Serge Ecoffey, Michel Pioro-Ladrière, Yann Beilliard, and Dominique Drouin. Analog programming of cmos-compatible al₂o₃/tio₂-x memristor at 4.2 k after metal-insulator transition suppression by cryogenic reforming. *Applied Physics Letters*, 123(16), October 2023. ISSN 1077-3118. doi:10.1063/5.0170058. URL <http://doi.org/10.1063/5.0170058>.
- [82] Raphaël Dawant, Matthieu Gaudreau, Marc-Antoine Roy, Pierre-Antoine Mouny, Matthieu Valdenaire, Pierre Gliech, Javier Arias Zapata, Malek Zegaoui, Fabien Alibert, Dominique Drouin, and Serge Ecoffey. Damascene versus subtractive line cmp process for resistive memory crossbars beol integration. *Micro and Nano Engineering*, 23:100251, June 2024. ISSN 2590-0072. doi:10.1016/j.mne.2024.100251. URL <http://doi.org/10.1016/j.mne.2024.100251>.
- [83] Xiao Xue, Bishnu Patra, Jeroen P. G. van Dijk, Nodar Samkharadze, Sushil Subramanian, Andrea Corna, Brian Paquelet Wuetz, Charles Jeon, Farhana Sheikh, Esdras Juarez-Hernandez, Brando Perez Esparza, Huzaifa Rampurwala, Brent Carlton, Surej Ravikumar, Carlos Nieva, Sungwon Kim, Hyung-Jin Lee, Amir Sammak, Giordano Scappucci, Menno Veldhorst, Fabio Sebastiano, Masoud Babaie, Stefano Pellerano, Edoardo Charbon, and Lieven M. K. Vandersypen. Cmos-based cryogenic control of silicon quantum circuits. *Nature*, 593(7858): 205–210, May 2021. ISSN 1476-4687. doi:10.1038/s41586-021-03469-4. URL <http://doi.org/10.1038/s41586-021-03469-4>.
- [84] Victor Yon, Frédéric Marcotte, Pierre-Antoine Mouny, Gebremedhin A. Dagnew, Bohdan Kulchitsky, Sophie Rochette, Yann Beilliard, Dominique Drouin, and Pooya Ronagh. A cryogenic memristive neural decoder for fault-tolerant quantum error correction. *ArXiv*, 2023. doi:10.48550/arxiv.2307.09463. URL <https://arxiv.org/abs/2307.09463>. Preprint.
- [85] Victor Yon, Bastien Galaup, Roger G. Melko, Yann Beilliard, and Dominique Drouin. Experimental online quantum dots charge autotuning using neural networks - output data, 2024. URL <https://zenodo.org/doi/10.5281/zenodo.13381665>.
- [86] Adam Paszke, Sam Gross, Francisco Massa, Adam Lerer, James Bradbury, Gregory Chanan, Trevor Killeen, Zeming Lin, Natalia Gimelshein, Luca Antiga, Alban Desmaison, Andreas Köpf, Edward Yang, Zach DeVito, Martin Raison, Alykhan Tejani, Sasank Chilamkurthy, Benoit Steiner, Lu Fang, Junjie Bai, and Soumith Chintala. Pytorch: An imperative style, high-performance deep learning library. *ArXiv*, 2019. doi:10.48550/arxiv.1912.01703. URL <https://arxiv.org/abs/1912.01703>. Preprint.

- [87] Diederik P. Kingma and Jimmy Ba. Adam: A method for stochastic optimization. *ArXiv*, 2014. doi:10.48550/arxiv.1412.6980. URL <https://arxiv.org/abs/1412.6980>. Preprint.
- [88] Lewis Smith and Yarín Gal. Understanding measures of uncertainty for adversarial example detection. *ArXiv*, 2018. doi:10.48550/arxiv.1803.08533. URL <https://arxiv.org/abs/1803.08533>. Preprint.
- [89] Chuan Guo, Geoff Pleiss, Yu Sun, and Kilian Q. Weinberger. On calibration of modern neural networks. *ArXiv*, 2017. doi:10.48550/arxiv.1706.04599. URL <https://arxiv.org/abs/1706.04599>. Preprint.
- [90] Juozas Vaicenavicius, David Widmann, Carl Andersson, Fredrik Lindsten, Jacob Roll, and Thomas B. Schön. Evaluating model calibration in classification. *ArXiv*, 2019. doi:10.48550/arxiv.1902.06977. URL <https://arxiv.org/abs/1902.06977>. Preprint.
- [91] Ethan Goan and Clinton Fookes. *Bayesian Neural Networks: An Introduction and Survey*, page 45–87. Springer International Publishing, 2020. ISBN 9783030425531. doi:10.1007/978-3-030-42553-1_3. URL http://doi.org/10.1007/978-3-030-42553-1_3.
- [92] Yongchan Kwon, Joong-Ho Won, Beom Joon Kim, and Myunghee Cho Paik. Uncertainty quantification using bayesian neural networks in classification: Application to biomedical image segmentation. *Computational Statistics & Data Analysis*, 142:106816, February 2020. ISSN 0167-9473. doi:10.1016/j.csda.2019.106816. URL <http://doi.org/10.1016/j.csda.2019.106816>.
- [93] Peter Auer. Using confidence bounds for exploitation-exploration trade-offs. *Journal of Machine Learning Research*, 3(Nov):397–422, 2002. URL <https://www.jmlr.org/papers/v3/auer02a.html>.
- [94] Alex Simpkins, Raymond de Callafon, and Emanuel Todorov. Optimal trade-off between exploration and exploitation. In *2008 American Control Conference*. Ieee, June 2008. doi:10.1109/acc.2008.4586462. URL <http://doi.org/10.1109/ACC.2008.4586462>.

Supplementary Materials: Experimental Online Quantum Dots Charge Autotuning using Neural Networks

S1 Datasets

The dataset [65] is built from nine offline stability diagrams measured during previous experiments on similar quantum dot (QD) devices. Each of them was manually annotated by experts with transition lines and charge regime areas (example in Figure 1c). The stability diagrams were decomposed into 33,429 patches of 18×18 pixels, then split into three subsets:

- 80 % training (26,743 patches): used to train the convolutional neural network (CNN) to detect transition lines.
- 10 % validation (3343 patches): used after training to select the step corresponding to the best model (shown as a green star in Figure S1).
- 10 % testing (3343 patches): used to evaluate the line classification accuracy after training.

Each patch is categorized as “*line*” if at least one transition line annotation intersects the 6×6 square at its center (pink squares in Figure S4a,b). This labeling approach provides more context to the neural network (NN) while keeping the classification window narrow enough to fit between two transition lines. Since the majority of the surface does not contain a line, only 8.6 % (3887) of the patches are categorized as “*line*”, while the others are classified as “*no-line*”.

S2 Model Training

The detection of transition lines is accomplished using CNNs containing 367,267 free parameters (weights and bias), structured as presented in Table S1 and trained with the meta-parameters presented in Table S2. We did not observe overfitting during training, as shown in Figure S1. Once trained, the model reached satisfactory performance on the test set (example in Figure S2), where most of the errors were related to ambiguous labels or noise patterns. The Python source code used for training and inference is available on *GitHub*¹ and relies on *PyTorch* [86].

The meta-parameters listed in Tables S1 and S2 were determined through a grid search and informed guesses. Some of them (input size, pixel size, and confidence threshold) are the result of a tradeoff between measurement time and classifier performance. While further optimization and fine-tuning of these parameters could improve the classification accuracy, exploration efficiency, and overall calibration success, the primary aim of this study is to demonstrate the feasibility of the autotuning procedure in an experimental setting rather than achieving optimal performance.

The training of a NN is partially stochastic due to the random initialization of the parameter values and mini-batch sampling during training. To avoid selection bias, in this study, we trained a new CNN using a different random seed for each autotuning run. In a production context, it is possible to train and use only one CNN to tune any device for a given QD technology.

Table S1: Architecture of the convolutional neural networks (CNNs) used to detect transition lines during the experiment. A simplified schematic of the layer structure is represented in Figure 1d.

Layer	Configuration
Input	18×18 pixels, 1 channel
Convolution 1	4×4 kernel, 6 channel
Convolution 2	4×4 kernel, 12 channel
Fully connected 1	200 neurons
Fully connected 2	100 neurons
Output	Binary classification (“ <i>line</i> ” or “ <i>no-line</i> ”) + uncertainty score

¹Python source code: github.com/3it-inpaqt/dot-calibration-v2

Table S2: Meta-parameters of the convolutional neural networks (CNNs) used for training and inference.

Meta-Parameter	Value
Number of train updates	30,000
Loss function	Binary cross-entropy
Optimizer	Adam [87]
Learning rate	0.001
Dropout	60 %
Batch size	512
Pixel size	4 mV
Confidence threshold	90 %

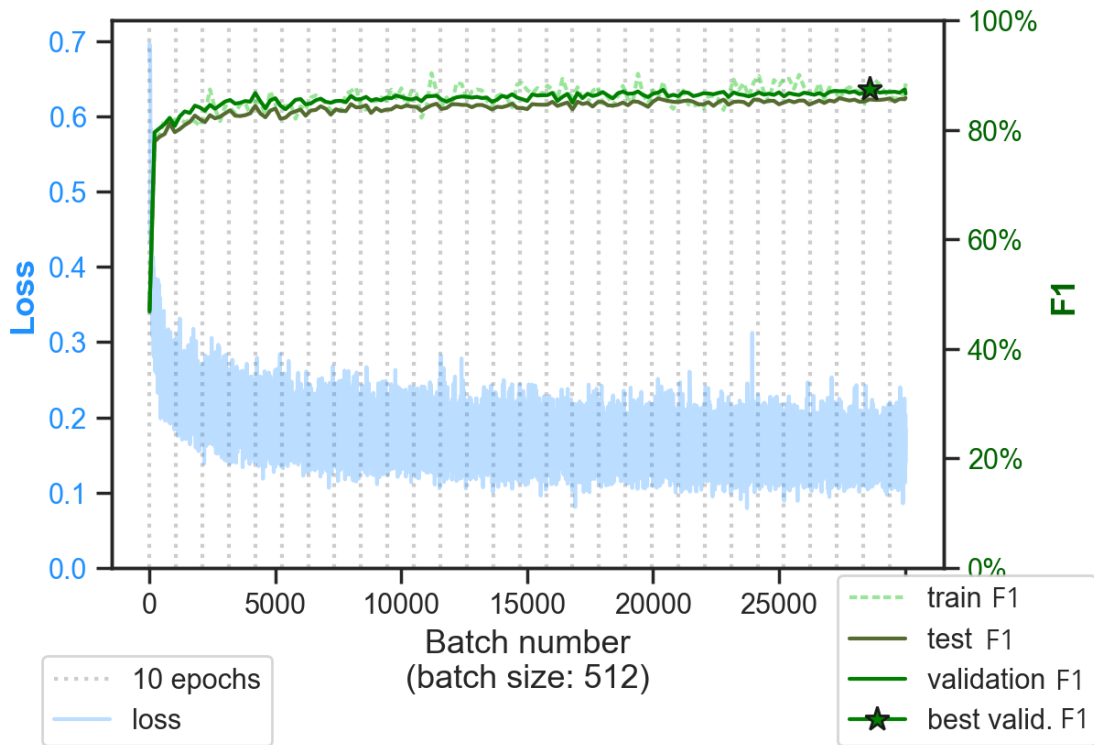


Figure S1: Example of convolutional neural network (CNN) training progress. The F1 score is the harmonic mean of precision and recall. The model performance quickly converges to a maximum, and no overfitting is visible.

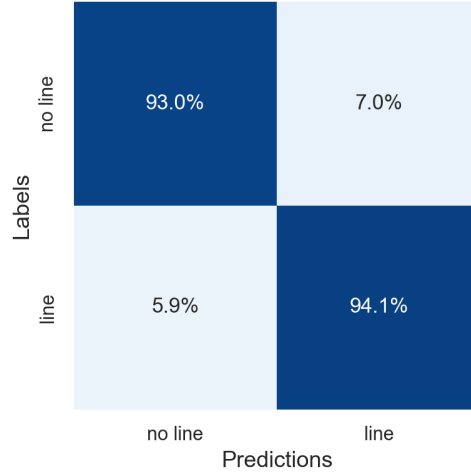


Figure S2: Example of a confusion matrix for a trained convolutional neural network (CNN). On the test set, this model obtained the following scores: accuracy, 93.09 %; precision, 80.88 %; recall, 93.52 %; F1 score, 85.56 %.

S3 Confidence Score

The confidence of model inference can be evaluated using several different methods [58, 88–92]. However, a previous study [51] has shown that, in the context of QD autotuning, a simple heuristic score based on the distance [75, 76] between the NN output (denoted as y) and the inferred class value (see Formula S1) is an efficient approximation of the model’s uncertainty. This confidence score is leveraged to increase the tuning success rate with minimal overhead time by optimizing the exploration–exploitation tradeoff [93, 94].

$$\text{Confidence score} = |0.5 - y| \times 2 \quad (\text{S1})$$

Based on offline tests, we empirically found that triggering the validation sequence if the confidence score was below 90 % provided a good tradeoff between the success rate and exploration time. Therefore, we used this value as a confidence threshold for the 20 online runs. This value could be optimized during future experiments.

S4 Autonomous Exploration Strategy

Each step of the exploration procedure (see Figure 2a) consists in (i) scanning a 18×18 square region in the voltage space (referred to as “patch”), (ii) processing it through a CNN-based line detection model, and (iii) determining the next region to explore.

The coordinates for the next exploration step are determined by a four-stage exploration strategy (see Figure S3):

1. **Search for the first transition line:** The algorithm explores the voltage space in four directions, forming an expanding “X” pattern by following the diagonals from the starting point. This stage is successfully completed when the first transition line is detected with a confidence level above the threshold.
2. **Estimate the line slope:** Patches are measured along two circular arcs centered on the first detected transition line. If the line is successfully located in both arcs, we use those two coordinates to estimate the slope of the line. If the line is not detected in one of the arcs, we keep the default slope value until the end of the procedure.
3. **Search for the empty regime:** The exploration proceeds in the two directions perpendicular to the estimated line slope. This stage is successfully completed when the empty regime is detected (i.e., no transition line detected for three times the average line distance in one direction) and at least five different transition lines are located.
4. **Locate the one-electron regime:** Using the estimated line slope, the average distance between lines, and the position of the first line after the empty regime, we infer the gate voltages corresponding to the one-electron regime.

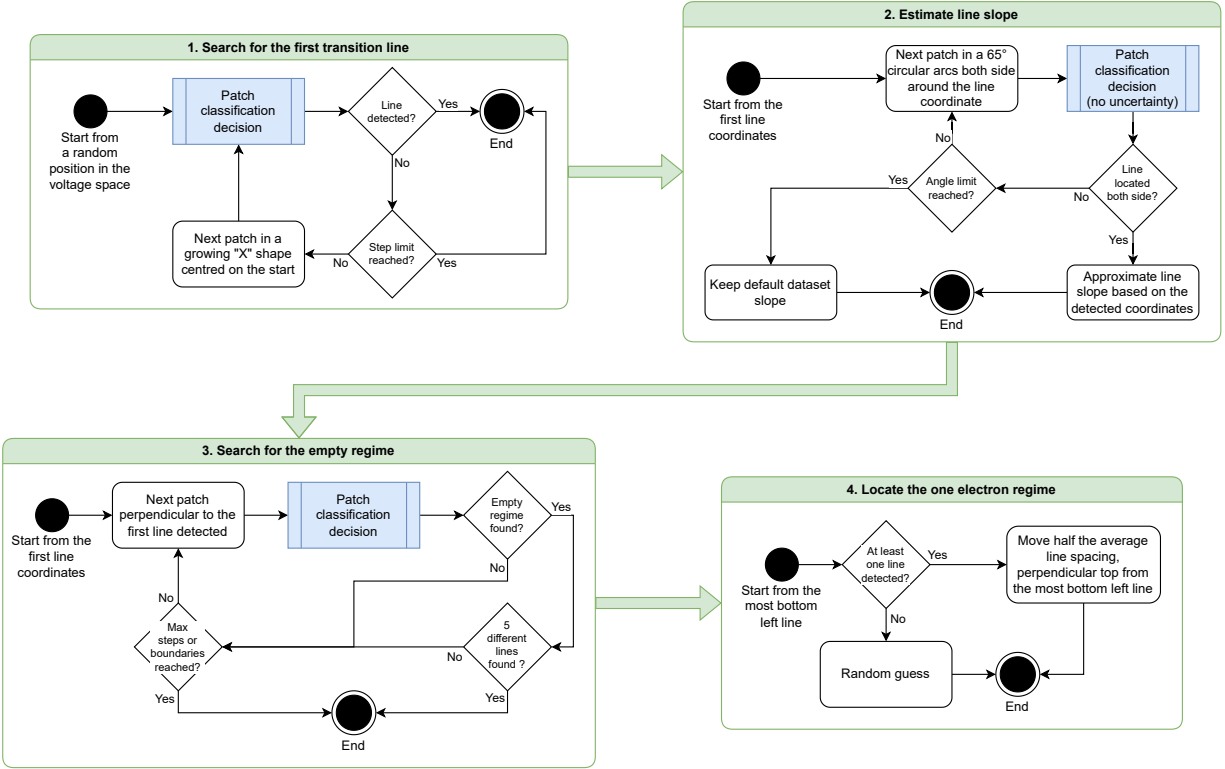


Figure S3: Flow diagram representing each stage of the autotuning exploration procedure.

The distance between two exploration steps is set to the width of the detection area (32 mV), except in the second step, where eight steps are distributed in a 65°-arc on each side. For further details on the exploration strategy and its benchmark on multiple offline datasets, see Yon et al. [51].

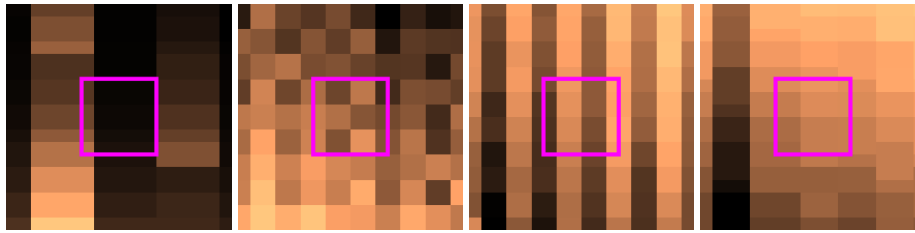
S5 Run Statistics

Table S3: Statistics and results of the 20 experimental runs.

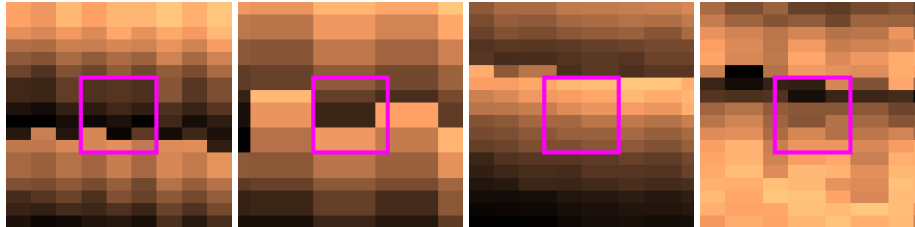
Run ID	#Steps	Measurement Time (s)	Processing Time (s)	Total Time (s)	Final Coord. (V, V)	Charge Regime
01	96	6,363	259	6,623	(-0.298, 0.840)	1
02	71	4,717	188	4,905	(0.135, 0.756)	1
03	88	5,860	234	6,094	(0.171, 0.760)	1
04	151	10,421	400	10,822	(-0.278, 0.828)	1
05	112	7,460	295	7,755	(-0.025, 0.796)	1
06	167	11,462	445	11,907	(-0.302, 0.840)	1
07	72	4,786	191	4,977	(-0.298, 1.196)	4+
08	69	4,670	182	4,852	(0.239, 0.760)	1
09	165	11,475	445	11,920	(-0.302, 0.828)	1
10	117	7,792	309	8,101	(0.175, 0.772)	1
11	76	5,090	211	5,301	(0.291, 0.740)	1
12	158	10,751	436	11,188	(0.440, 0.752)	1
13	116	7,694	305	7,998	(0.151, 0.776)	1
14	160	11,138	429	11,567	(-0.302, 0.836)	1
15	80	5,299	211	5,510	(-0.298, 0.840)	1
16	89	5,917	236	6,153	(-0.089, 0.792)	1
17	116	7,790	311	8,101	(-0.085, 0.808)	1
18	62	4,127	166	4,293	(-0.005, 0.784)	1
19	75	5,063	200	5,263	(-0.194, 0.812)	1
20	169	11,737	457	12,195	(-0.302, 0.828)	1

S6 Patch Measurement Examples

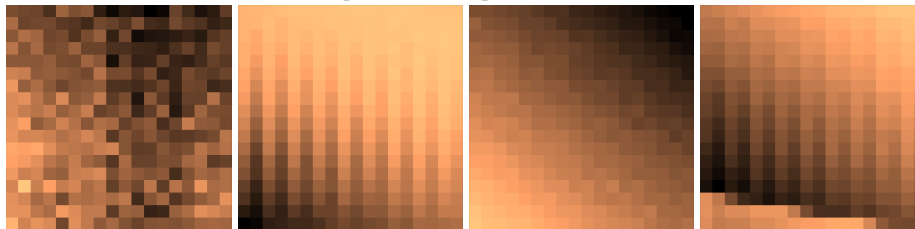
It was necessary to interpolate the images of the offline stability diagrams before using them to train the CNNs due to the variable sweeping step size used during the original experiments. This preprocessing slightly affected the quality of the offline training by duplicating some pixels (see patch examples in Figure S4a,b). On the other hand, the patches measured during the online experiment did not suffer from this limitation, as it was possible to define the desired step size in the measurement interface. This led to a better resolution of the patch, with clearer lines (see patch examples in Figure S4c,d).



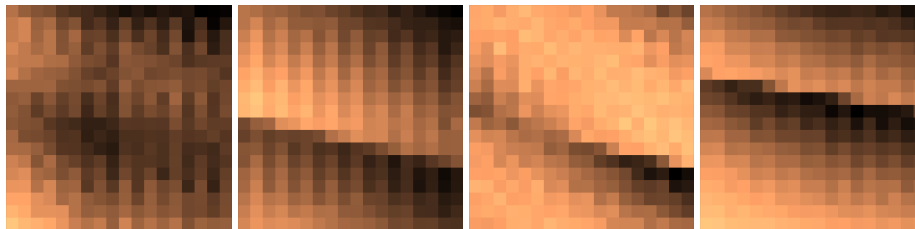
(a) Four examples of offline patches labeled as “no-line”.



(b) Four examples of offline patches labeled as “line”.



(c) Four examples of online patches correctly classified as “no-line”.



(d) Four examples of online patches correctly classified as “line”.

Figure S4: Patch samples for each class from the offline training set and the online experiment. **a,b)** The patches are measured using variable step sizes depending on the stability diagram, then interpolated at 4 mV per pixel. A patch is labeled as “line” only if a transition line annotation intersects with the detection area (highlighted in pink) at its center. **c,d)** The online patches are measured using a step size of 4 mV per pixel.